npj | clean water

Article

Published in partnership with King Fahd University of Petroleum & Minerals

https://doi.org/10.1038/s41545-024-00316-7

The photocatalytic oxidation of As(III) on birnessite

Ping Li[1,2,3], Yun Wang[1,2], Jingjing Wang[1,2], Wei Wang[1,2], Zhe Ding[1,2,3], Jianjun Liang[1,2,3] & Qiaohui Fan[1,2,3]

Birnessite is regarded as an efficient oxidizing agent that would significantly influence the environmental fate of elements such as arsenic. This study compared the chemical and photocatalytic oxidation of As(III) over birnessite. During the chemical oxidation, As(III) was oxidized to As(V), while Mn(IV) was reduced to Mn(II), subsequently forming MnOOH. The coverage of the reactive sites by MnOOH inhibited the chemical oxidation of residual As(III). At pH 5.0, after 360 min of reaction, 61% of As(III) was oxidized to As(V), and the oxidation of As(III) decreased with an increase in pH. The photocatalytic oxidation of As(III), where almost all As(III) could be oxidized to As(V) over a pH range of 5.0–8.0 and 360 min, was much more efficient compared to chemical oxidation. In contrast to chemical oxidation, the formation of MnOOH slightly affected the photocatalytic performance of birnessite. It was demonstrated that $\bullet O_2^-$ radicals and holes (h_{vb}^+) played an important role in the photocatalytic oxidation of As(III) over birnessite. Our findings confirmed that light dramatically promoted the oxidation of As(III) by birnessite, broadening the understanding of the environmental behaviors of arsenic.

Arsenic is a component of over 245 minerals in the crust of the earth, and has attracted considerable attention in recent years owing to its high toxicity and carcinogenicity[1–4]. Arsenite and arsenate are the predominant inorganic arsenic species in natural aqueous systems. Aqueous arsenite primarily occurs as $H_2AsO_3^-$ and H_3AsO_3, whereas arsenate primarily occurs as $H_2AsO_4^-$ and $HAsO_4^{2-}$ species in the environment[5–7]. Owing to the high affinity between As(III) and the sulfhydryl groups in proteins, the toxicity of As(III) is approximately 25 to 60 times higher than that of As(V)[1,8–10]. Furthermore, As(III) is poorly adsorbed by minerals compared to As(V), consequently, it has greater mobility in the environment[9,10]. Therefore, the environmental fate of As closely depends on its chemical state, and the alteration of its chemical state in the environment should be among the primary concerns. It has been reported that As(III) can be oxidized to As(V) by natural minerals or under certain oxidation conditions[11–14]. Therefore, it is necessary to comprehensively consider the transformation of the chemical state of As on the surface of natural minerals to better understand the environmental behavior of arsenic.

Birnessite is widely distributed in soils, sediments, aquifers, oceans, rivers, and lakes[15], and plays a significant role in the natural environment due to its redox properties[16]. Birnessite has been reported to oxidize Co(II), Cr(III), V(IV), Pu(IV) and Se(IV) to their higher valences[17–21], thereby playing an important role in tuning the chemical state and, subsequently, the behaviors of these elements in the natural environment. Therefore, the oxidative nature of birnessite has attracted considerable attentions. Besides the chemical oxidation ability, it is well known that birnessite has a moderate bandgap (1.8–2.7 eV)[22–25], and could induce strong redox reactions upon light irradiation. Birnessite (based) photocatalysts have been widely applied for the photocatalytic degradation of CO oxidation[26], organic pollutants[27–30], and water splitting[25]. However, as a naturally occurred semiconductor, its photocatalytic activity in natural environment is sometimes ignored[31]. Generally, semiconductor minerals would significantly influence the chemical states and species of adjacent elements and organic matter[32,33], subsequently alerting their environmental fate. It has been demonstrated that As(III) is easily converted to As(V) on light-irradiated semiconductor minerals such as TiO_2, goethite, and ferrihydrite[6,7,34,35]. Shumlas et al.[11] reported the enhanced oxidation of As(III) on birnessite under light. However, the effects of natural semiconductors on arsenic environmental behavior remains relatively lacking. Therefore, a comprehensive investigation on the chemical oxidation and photocatalytic oxidation of As(III) by semiconductor minerals like birnessite is needed.

The objective of this study is to reveal the adjustment of the chemical states of arsenic by birnessite. This study performs a detailed investigation of

[1]Northwest Institute of Eco-Environment and Resources, Chinese Academy of Sciences, Lanzhou 730000, China. [2]Key Laboratory of Petroleum Resources Exploration and Evaluation, Gansu Province, Lanzhou 730000, China. [3]Key Laboratory of Strategic Mineral Resources of the Upper Yellow River, Ministry of Natural Resources, Lanzhou 730000, China. e-mail: fanqh@lzb.ac.cn

the chemical and photocatalytic oxidation of As(III) by birnessite, and discusses the mechanisms of the oxidation of As(III). This is expected to provide more insight into the geochemistry of As in the environment and encourage further investigations of the light-assisted oxidation of As(III) by semiconductor minerals.

Results and discussion

Chemical oxidation of As(III) on birnessite

Figure 1a depicts the chemical oxidation of As(III) by birnessite at different pH under dark conditions. Owing to the presence of structural Mn^{4+}, which has strong oxidative abilities, As(III) was gradually oxidized by birnessite to produce As(V). In contrast, As(III) was barely converted to As(V) in the absence of birnessite (Supplementary Fig. 1). It is noteworthy that the oxidation of As(III) decreased after reaction period of approximately 360 min, and almost no additional As(V) was produced. After reaction for 360 min, ~72% of As(III) was converted to As(V) at pH 5.0. However, less As(III) was oxidized at higher pH, and the oxidation rates of As(III) were 59% and 54% at pH 6.5 and 8.0, respectively. These phenomena could be attributed to the formation of MnOOH on the birnessite surface during reaction with As(III)[11,36]. The detailed reaction is as follows:

$$2MnO_2 + AsO_3^{3-} + H_2O \rightarrow 2MnOOH + AsO_4^{3-} \quad (1)$$

Owing to the formation of MnOOH on the surface, the reactive sites on birnessite for oxidizing As(III) were covered. Therefore, the oxidation of As(III) by birnessite decreased as the reaction progressed. It was reported that the oxidation of As(III) by Mn(IV) produced Mn(II), which subsequently led to the generation of MnOOH[37]. Since these two processes were facilitated at low pH[36], more As(V) was generated at low pH. In addition, Supplementary Fig. 2 showed that MnOOH would be more stable at high pH, and the further oxidation of As(III) should be more difficult.

To demonstrate the passivation of birnessite surface by MnOOH, the chemical states of Mn in birnessite before and after oxidizing As(III) were compared. As shown in Supplementary Fig. 3, compared with raw birnessite, the binding energy of Mn 2p and 3 s shifted lower after eacting with As(III), indicating the reduction of Mn(IV). The content of Mn(III) obviously increased after reacting with As(III) (Supplementary Fig. 4). As shown in Supplementary Fig. 5, after reaction with As(V), the Mn K-edge shifted toward lower energy and located between MnOOH and birnessite, indicating a decrease of the average Mn oxidation state[38]. The crystal structures of the samples were obtained by XRD, as shown in Fig. 1b. The peaks at 12.4° and 24.9° were assigned to the (001) and (002) facets of birnessite, respectively. However, after reaction with As(III), an additional peak appeared at 26.2°, which is the characteristic of the (11-1) facet of manganite (MnOOH, PDF# 41-1379)[36]. Owing to the conversion of birnessite to MnOOH, the crystallinity of birnessite decreased and led to the broadening of the peaks. To further verify the formation of manganite, TEM was employed to compare the morphology of the birnessite surface (Fig. 1c). The microcosmic observation elucidates that more folds formed at the edge of birnessite after oxidizing As(III), and many black spots with a size of ~1.5 nm could be observed on reacted birnessite. This indicates the formation of new minerals. By further analyzing the high-resolution TEM

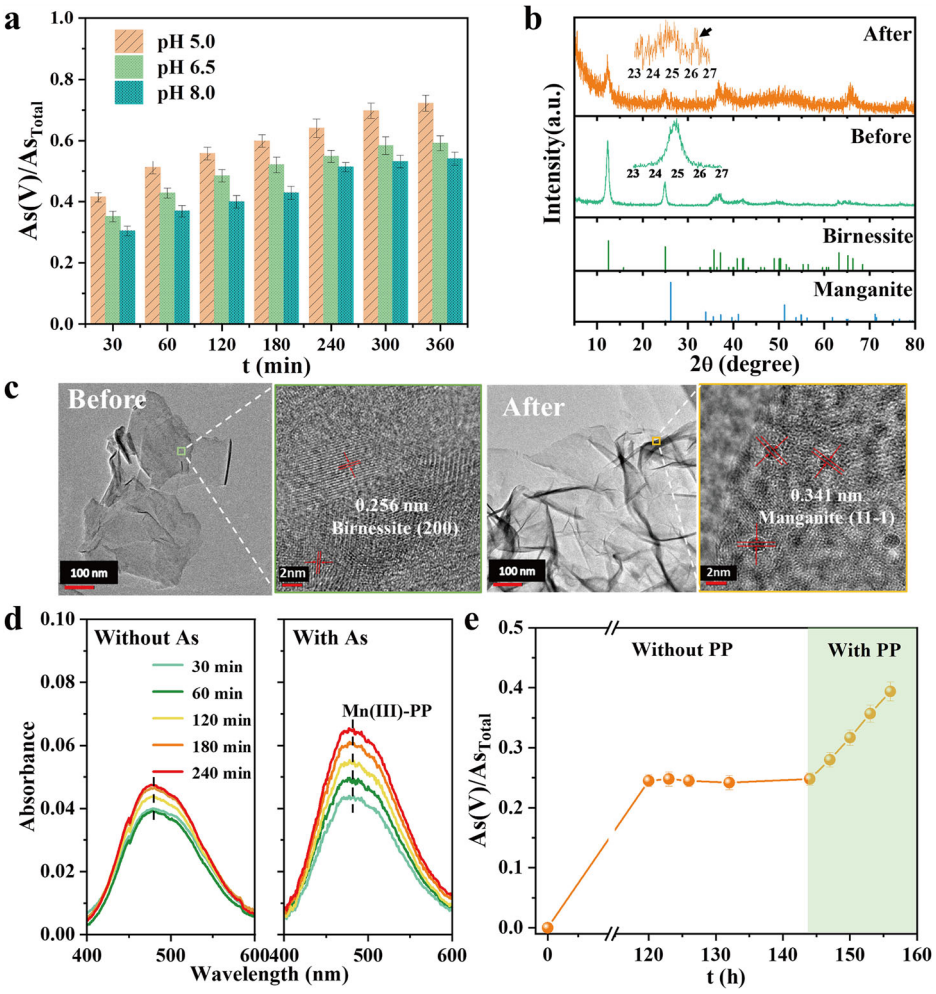

Fig. 1 | Interaction of As(III) with birnessite in darkness. The chemical oxidation of As(III) by birnessite at different pH (**a**); X-ray powder diffraction (XRD) patterns of birnessite before and after As(III) oxidation (**b**); Transmission electron microscopy (TEM) and high-resolution TEM (HRTEM) images of birnessite before and after As(III) oxidation (**c**); UV-vis absorption spectra of formed Mn(III)-PP species before and after As(III) oxidation (**d**); and effects of pyrophosphate (PP) on As(III) chemical oxidation by birnessite (**e**) Each experiment was duplicated, and data are presented as mean values ± standard deviations.

(HRTEM) images, it was found that the interference fringe spacing of the newly formed mineral on the birnessite surface was 0.341 nm, which corresponded to the (11-1) plane of manganite. This was obviously different from that observed on raw birnessite (0.256 nm, (200) plane). Together, these results demonstrate the formation of MnOOH on the birnessite surface after oxidizing As(III).

To verify the negative effect of MnOOH on the oxidation of As(III), pyrophosphate (PP) was employed as a chelating agent for Mn(III) to inhibit the formation of MnOOH on birnessite via the following reaction[36,39,40]:

$$MnOOH + HP_2O_7^{3-} + 3H^+ = MnHP_2O_7 + 2H_2O \quad (2)$$

As shown in Fig. 1d, the characteristic absorption band of the Mn(III)-PP complex at 480 nm[41] increased upon increasing the reaction time with As(III). This indicates that Mn(III) was released during the oxidation of As(III) by birnessite. In contrast, a slight increase in the amount of released Mn(III) was detected for raw birnessite, where Mn(III) mainly origins from the defects in birnessite[16]. Further using birnessite to oxidize As(III) with high concentration (50.0 mg/L), the surface of birnessite was completely passivated and the oxidation of As(III) stopped after reaction for 120 h, where only 25% of As(III) was oxidized (Fig. 1e). Although the oxidation of As(III) by birnessite was completely inhibited, the presence of PP resulted in the production of more As(V) (Fig. 1e). Hence, it can be concluded that As(III) can be chemically oxidized by birnessite to a certain extent. However, the gradual formation of MnOOH on the surface would restrain further oxidation of the remaining As(III), thereby causing the 'self-repression' effect.

Photocatalytic oxidation of As(III) over birnessite

To evaluate the oxidation of As(III) under light irradiation, the As(III) solution was irradiated in the absence of birnessite, and no As(V) was produced (Supplementary Fig. 6). It confirmed that the photocatalytic oxidation of As(III) did not occur in the absence of birnessite. Figure 2a shows the photocatalytic oxidation of As(III) over birnessite at different pH values. Compared with the chemical oxidation of As(III) in the dark, the oxidation of As(III) under light was considerably more efficient, and 100% of As(III) was converted to As(V) within 360 min at pH 6.5 and 8.0. The reaction rate constants (k) calculated using the pseudo first-order model[42,43] are shown in Supplementary Fig. 7. The oxidation rates of As(III) under light were 2.61, 5.65 and 7.61 times higher than the chemical oxidation of As(III) at pH 5.0, 6.5, and 8.0, respectively. Therefore, the enhanced oxidation of As(III) was considered to be closely related to the photocatalytic reactions induced by light-irradiated birnessite. Typically, birnessite is regarded as a naturally occurring semiconductor, which exhibited excellent ability for light absorbance (Supplementary Fig. 8). Under visible light irradiation, electrons in the valence band (e_{cb}^-) were excited to the conduction band. The photo-induced electrons together with the holes left in the valance band (h_{vb}^+), and induced radicals cause redox reactions. EPR experiments were performed to investigate the production of radicals. As shown in Fig. 2b, the signals of •OH and $•O_2^-$ adducts were clearly observed upon light irradiation, and more $•O_2^-$ was generated than •OH radicals in this system. According to the XPS valence band (VB) (Supplementary Fig. 9), the VB potential of birnessite was calculated to be 1.68 eV using the equation $E_{NHE} = \Phi + E_{VBM} - 4.44$, where the work function $\Phi = 4.00$ eV. It is too low to produce •OH radicals by oxidating water or OH^-. Therefore, the low concentrations of •OH was derived from the reduction of $•O_2^-$ radicals[44]. For As(III), it was demonstrated that h_{vb}^+, $•O_2^-$, •OH, and H_2O_2 can act as the reactive oxidative species (ROS) to oxidize As(III)[11,45–47]. To verify the dominant ROS for As(III) oxidation in the present study, radical trapping experiments were conducted, where mannitol, benzoic acid, p-benzoquinone, and catalase were used as scavengers for h_{vb}^+, •OH, $•O_2^-$, and H_2O_2, respectively. Figure 2c shows that the presence of benzoic acid and catalase in the catalytic system did not have a noticeable effect on the oxidation of As(III). In contrast, significant inhibition was observed after the introduction of p-benzoquinone and mannitol. These results indicated that $•O_2^-$ and h_{vb}^+ acted as the main ROS for the photocatalytic As(III) oxidation on birnessite.

The proposed processes for the photocatalytic oxidation of As(III) to As(V) are shown in Eqs. (3)–(6):

$$MnO_2 + hv = hvb^+ + e_{cb}- \quad (3)$$

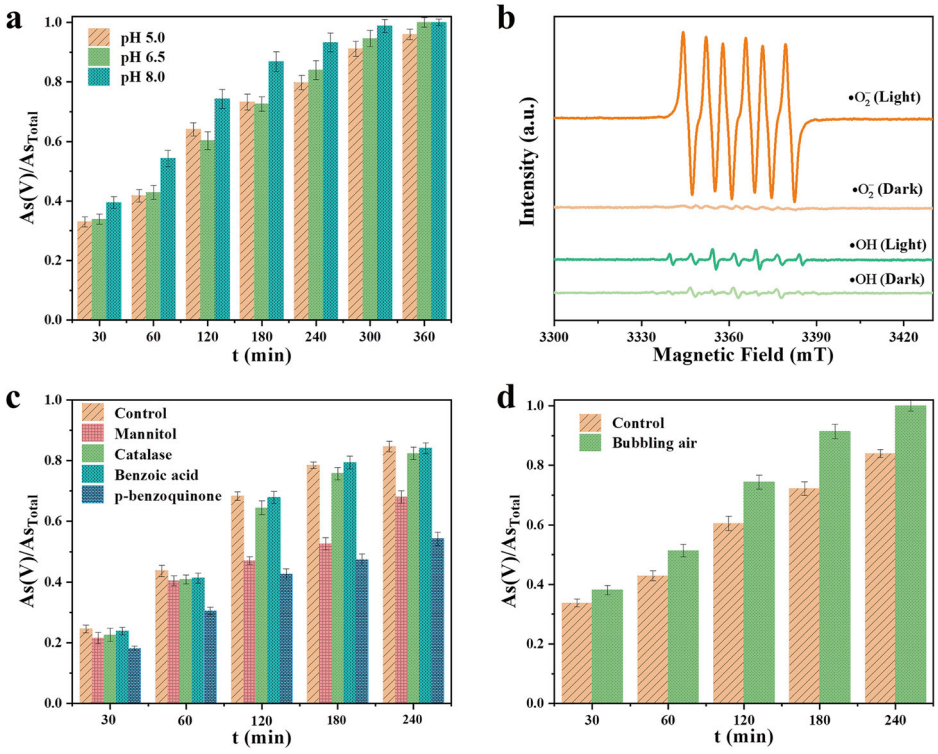

Fig. 2 | Oxidation of As(III) by birnessite under light. The photocatalytic oxidation of As(III) at different pH (**a**); electron paramagnetic resonance (EPR) spectra of radical adducts trapped by DMPO (•OH and $•O_2^-$) in dark conditions and under visible light irradiation (**b**); free radical capture experiments: mannitol, catalase, benzoic acid, and p-benzoquinone were used as scavengers of h_{vb}^+, H_2O_2, •OH, and $•O_2^-$, respectively (**c**); and effect of O_2 on photocatalytic oxidation of As(III) (**d**). Each experiment was duplicated, and data are presented as mean values ± standard deviations.

$$As(III) + 2h_{vb}^{+} = As(V) \quad (4)$$

$$O_2 + e_{cb}^{-} = \bullet O_2 - \quad (5)$$

$$As(III) + \bullet O_2^{-} = As(V) \quad (6)$$

It has been proved that h_{vb}^{+} was the main ROS for the photocatalytic oxidation of As(III) by birnessite[11]. However, in this study, $\bullet O_2^{-}$ also played a key role in oxidating As(III). As the generation of $\bullet O_2^{-}$ radicals is closely related to the capture of electrons by oxygen molecules, the oxidation of As(III) was further conducted by bubbling air. As expected, the system purged with air showed a higher rate of As(III) oxidation than the system purged without air (Fig. 2d). Nevertheless, the bubbling air in the system did not cause an obvious change in the chemical oxidation of As(III) in the dark conditions (Supplementary Fig. 10). This further demonstrated that $\bullet O_2^{-}$ radicals acted as the ROS in the photooxidation of As(III) over birnessite.

Mechanism for enhancement of As(III) oxidation under light irradiation

Our findings elucidated that the formation of MnOOH could lead to the passivation of the birnessite surface. This resulted in the coverage of active sites, and subsequently inhibited the further oxidation of As(III) in the dark. In contrast to chemical oxidation, the oxidation of As(III) under light was much more efficient. In particular, even when the chemical oxidation of As(III) stopped due to the passivation of birnessite, it still exhibited excellent photocatalytic oxidation performance for As(III) upon light irradiation (Fig. 3a). As shown in Supplementary Fig. 11, MnOOH did not show photocatalytic activity for the oxidation of As(III). The photoelectric properties of birnessite before and after the formation of MnOOH on the catalyst surface were compared to understand the mechanism responsible for the enhanced photocatalytic performance of birnessite in As(III) oxidation. As shown in the inset in Fig. 3b, the photocurrent intensity of raw birnessite was 1.25 μA cm^{-2}, which was close to that of reacted birnessite (1.20 μA cm^{-2}). This was further confirmed by the Nyquist plot obtained from electrochemical impedance spectroscopy (EIS), where a similar semicircle radius was observed. This suggests that the resistances at the interface of the semiconductor and electrolyte were almost the same. Mott-Schottky plots were employed to investigate the electronic band structure of birnessite before and after the reaction (Fig. 3c). The flat band potential of raw birnessite is (− 0.91 V vs. SCE), which is close to that of birnessite after reaction (− 0.88 V vs. SCE). The valence band X-ray photoelectron spectroscopy (inset in Fig. 3c) also clearly show that the VB of birnessite did not change after oxidating As(III). Moreover, birnessite showed emission over the range of 400–600 nm in the photoluminescence (PL) spectrum, and it hardly changed after oxidating As(III) (Supplementary Fig. 12). This indicates that the separation rate of the photo-generated charge carriers on birnessite was hardly influenced by the generated MnOOH. These results demonstrated that the formation of MnOOH on the birnessite surface did not bring obviously negative effect to the band structure or the photoelectric properties of birnessite. EPR spectra (Fig. 3d) showed that, similar to raw birnessite, $\bullet O_2^{-}$ radicals were also generated on MnOOH loaded birnessite, which would act as the ROS for oxidizing As(III) to As(V). This clearly explains why the light-induced photocatalytic reactions showed much higher reactivity for the oxidation of As(III) than chemical oxidation.

As illustrated in Fig. 4, the oxidation of As(III) by birnessite is summarized as follows: (1) In the dark, structural Mn(IV) would directly oxidize As(III) to As(V). During this process, Mn(IV) was reduced, and the released Mn(II) induced the formation of MnOOH on the birnessite surface. The coverage of reactive sites by MnOOH inhibited the further oxidation of residual As(III). (2) Upon light irradiation, birnessite could act as a natural semiconductor and induce redox reactions, and the photogenerated $\bullet O_2^{-}$ radicals and h_{vb}^{+} acted as the ROS for oxidizing As(III). Although MnOOH was also formed on the mineral surface, the photocatalytic properties of birnessite were unaffected. Thus, the oxidation of As(III) by birnessite under light showed much higher reactivity than chemical oxidation in the dark.

Environmental implications

The results above verified the important role of birnessite in the oxidation of As(III). In particular, light irradiation significantly promoted the oxidation of As(III) to As(V), thereby significantly reducing the toxicity and hazards of As. Furthermore, the uptake of As(V) by natural media is much easier than that of As(III)[48–50]. To further verify the environmental implication of these findings, the oxidation of As(III) was tested with naturally-occurring

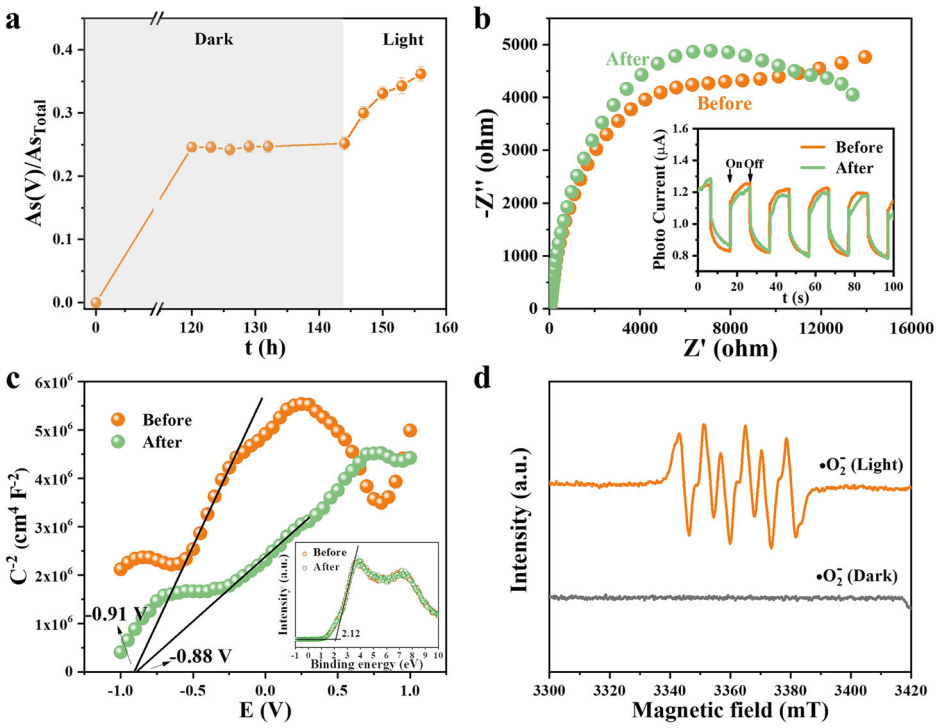

Fig. 3 | Effect of MnOOH on the photocatalytic performance of birnessite. Effect of light on As(III) oxidation by birnessite (**a**); optical properties of birnessite after the photocatalytic reactions: photocurrent response spectra (inset) and electrochemical impedance spectroscopy (EIS) (**b**); electrochemical Mott-Schottky plots (**c**); and EPR spectra of radical adducts trapped by DMPO ($\bullet O_2^{-}$) (**d**). Each experiment was duplicated, and data are presented as mean values ± standard deviations.

manganese oxide ore, which contains birnessite (Supplementary Fig. 13). Figure 5a shows that ~25% of As(III) was chemically oxidized to As(V) by this birnessite-containing mineral in darkness. In sharp contrast, ~70% of As(III) was converted to As(V) under light irradiation. Therefore, light-irradiated birnessite would significantly impact the species of As, and subsequently change its environmental fate, owing to the widespread nature of birnessite. This would help improve the understanding and assessment of the environmental behavior of arsenic.

In addition, the excellent photocatalytic performance of birnessite for the oxidation of As(III) is expected to be useful for reducing the difficulty of the treatment of arsenite-containing wastewater. For instance, wastewater produced by copper smelteries contains high concentrations of arsenite and heavy metals[51,52] (Supplementary Table 1). When birnessite was used as the oxidation reagent, all As(III) was adsorbed in the presence of coexisting cations. As shown in Fig. 5b, only 13% of As(III) was oxidized to As(V) by birnessite in the dark. In contrast, the oxidation of As(III) to As(V) rapidly occurred under light irradiation, and approximately all As(III) (more than 93%) was converted to As(V) after 12 h. Therefore, the photocatalytic method is an excellent and effective strategy for treatment of arsenite-containing wastewater. Furthermore, some specific natural minerals, such as tailings of manganese ore, may be used as catalysts for the treatment of arsenite waste and the remediation of arsenite pollution. Comparing with other artificial catalyst, natural birnessite-containing minerals are easy to obtain and was economical and environment-friendly. More importantly, it could provide continuous oxidation ability for As(III) day and night.

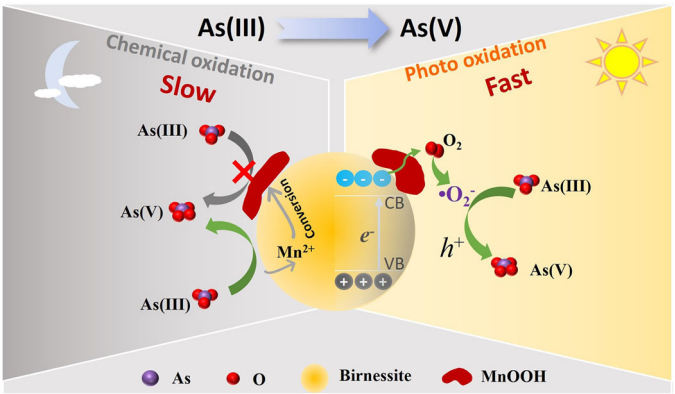

Fig. 4 | Schematic diagram of As(III) oxidation by birnessite. The chemical oxidation in darkness and the photocatalytic oxidation under light irradiation.

Methods

Preparation of birnessite

All chemicals used in this experiment were of analytical grade and were used without further treatment. Birnessite was synthesized using a one-pot synthesis method[53]. Briefly, 1.352 g $MnSO_4{\cdot}H_2O$ and 2.992 g EDTA-Na were added to 25 mL of deionized water, and the suspension was stirred for 30 min. Subsequently, 1.2 mol/L NaOH was added slowly at a rate of 3.0 mL/min. During this process, the color of the solution changed gradually until a black precipitate appeared. The final suspension was stirred for an additional two hours. The resulting solid was filtered and washed several times with deionized water to remove residual ions. Finally, the product was dried in a freeze dryer. The natural manganese oxide ore was commercially obtained from Honghu Mineral Co., ltd. The methods for the characterization of the samples can be found in the Supplementary Information.

Photocatalytic and chemical oxidation of As(III)

All experiments were conducted in a 25 mL quartz tube. Birnessite (9.0 mg) was suspended in 14.85 mL deionized water, and 0.15 mL of 1.0 g/L As(III) was added to the suspension. To achieve the relatively complete passivation of birnessite surface, 50.0 mg/L As(III) was used in some systems. The pH of the suspension was adjusted with 0.1 mol/L NaOH or HCl solution. The aqueous suspensions were then illuminated using a 300 W Xe lamp equipped with a 380 nm filter. At the desired time intervals, a 2.0 mL aliquot of the suspension was collected and then separated using a 0.22 μm filter membrane prior to analysis by ion chromatography (IC, ICS-600, Metrohm). As it is proven that As(V) was hardly adsorbed by birnessite (Supplementary Fig. 1), the detected As(V) in the solution was considered to be that produced by oxidation of As(III). For comparison, the chemical oxidation of As(III) was conducted in the absence of light irradiation.

To evaluate the generation of Mn(III), 20 mg/L pyrophosphate (PP) was added into the chemical oxidation system to chelate Mn(III). The concentration of Mn(III)-PP complexes in the supernatant was measured using a UV-vis spectrophotometer (Unico UV-2600).

Detection of reactive oxidative species

The reactive oxidative species (ROS) for the oxidation of As(III) were measured via trapping experiments, in which mannitol (20 mmol/L), catalase (3000 units/mL), p-benzoquinone (2 mmol/L), and benzoic acid (20 mmol/L) were added as scavengers for h_{vb}^+, H_2O_2, $\bullet O_2^-$ radicals, and •OH radicals, respectively. All trapping experiments were conducted at pH 6.5 and the

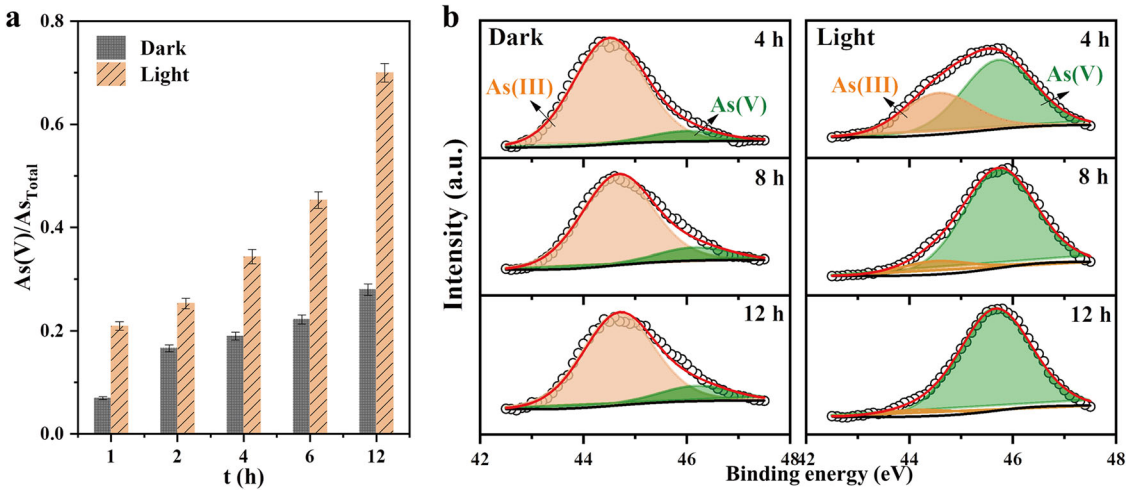

Fig. 5 | Application of the photocatalytic As(III) oxidation. The oxidation of As(III) by natural manganese oxide ore (**a**); Change of the As 3d spectra of As in simulated wastewater in the presence of birnessite in darkness and under light irradiation (**b**). Each experiment was duplicated, and data are presented as mean values ± standard deviations.

As(V) produced was measured by IC. As well, electron paramagnetic resonance (EPR) spectroscopy was adapted to the measurement of ROS.

Data availability

The data sets generated during and/or analyzed during the current study are available from the corresponding author on reasonable request.

Received: 26 May 2023; Accepted: 11 March 2024;
Published online: 19 March 2024

References

1. Mandal, B. K. & Suzuki, K. T. Arsenic round the world: a review. *Talanta* **58**, 201–235 (2002).
2. Hettick, B. E., Cañas-Carrell, J. E., French, A. D. & Klein, D. M. Arsenic: a review of the element's toxicity, plant interactions, and potential methods of remediation. *J. Agric. Food Chem.* **63**, 7097–7107 (2015).
3. Chen, Q. Y. & Costa, M. Arsenic: a global environmental challenge. *Annu. Rev. Pharmacol. Toxicol.* **61**, 47–63 (2021).
4. Hu, S., Yan, L., Chan, T. & Jing, C. Molecular insights into ternary surface complexation of arsenite and cadmium on TiO_2. *Environ. Sci. Technol.* **49**, 5973–5979 (2015).
5. Akter, K. F., Owens, G., Davey, D. E. & Naidu, R. Arsenic speciation and toxicity in biological systems. *Rev. Environ. Contam. Toxicol.* **184**, 97–149 (2005).
6. Bhandari, N., Reeder, R. J. & Strongin, D. R. Photoinduced oxidation of arsenite to arsenate on ferrihydrite. *Environ. Sci. Technol.* **45**, 2783–2789 (2011).
7. Bhandari, N., Reeder, R. J. & Strongin, D. R. Photoinduced oxidation of arsenite to arsenate in the presence of goethite. *Environ. Sci. Technol.* **46**, 8044–8051 (2012).
8. Singh, R., Singh, S., Parihar, P., Singh, V. P. & Prasad, S. M. Arsenic contamination, consequences and remediation techniques: a review. *Ecotox. Environ. Safe* **112**, 247–270 (2015).
9. Korte, N. E. & Fernando, Q. A review of arsenic(III) in groundwater. *Crit. Rev. Environ. Sci. Technol.* **21**, 1–39 (1991).
10. Wang, C. et al. Removal of As(III) and As(V) from aqueous solutions using nanoscale zero valent iron-reduced graphite oxide modified composites. *J. Hazard. Mater.* **268**, 124–131 (2014).
11. Shumlas, S. L. et al. Oxidation of arsenite to arsenate on birnessite in the presence of light. *Geochem. Trans.* **17**, 1–10 (2016).
12. Neppolian, B., Celik, E. & Choi, H. Photochemical oxidation of arsenic(III) to arsenic(V) using peroxydisulfate ions as an oxidizing agent. *Environ. Sci. Technol.* **42**, 6179–6184 (2008).
13. Katsoyiannis, I. A., Zouboulis, A. I. & Jekel, M. Kinetics of bacterial As(III) oxidation and subsequent As(V) removal by sorption onto biogenic manganese oxides during groundwater treatment. *Ind. Eng. Chem. Res.* **43**, 486–493 (2004).
14. Yang, H., Sun, W., Ge, H. & Yao, R. The oxidation of As(III) in groundwater using biological manganese removal filtration columns. *Environ. Technol.* **36**, 2732–2739 (2015).
15. Ling, F. T. et al. A multi-method characterization of natural terrestrial birnessites. *Am. Mineral.* **105**, 833–847 (2020).
16. Peng, H. et al. Redox properties of birnessite from a defect perspective. *Proc. Natl. Acad. Sci. USA.* **114**, 9523–9528 (2017).
17. Crowther, D. L., Dillard, J. G. & Murray, J. W. The mechanisms of Co(II) oxidation on synthetic birnessite. *Geochim. Cosmochim. Acta* **47**, 1399–1403 (1983).
18. Scott, M. J. & Morgan, J. J. Reactions at oxide surfaces. 2. Oxidation of Se(IV) by synthetic birnessite. *Environ. Sci. Technol.* **30**, 1990–1996 (1996).
19. Rajapaksha, A. U., Vithanage, M., Ok, Y. S. & Oze, C. Cr(VI) formation related to Cr(III)-muscovite and birnessite interactions in ultramafic environments. *Environ. Sci. Technol.* **47**, 9722–9729 (2013).
20. Zhao, P., Johnson, M. R., Roberts, S. K., Zavarin, M. Np and Pu sorption to manganese oxide minerals; report No.: UCRL-TR-214984; U. S. Department of Energy, National Nuclear Security Administration, Nevada Site Office; https://www.osti.gov/servlets/purl/883729-rcaqD8/ (2005).
21. Abernathy, M. J., Schaefer, M. V., Vessey, C. J., Liu, H. & Ying, S. C. Oxidation of V(IV) by birnessite: kinetics and surface complexation. *Environ. Sci. Technol.* **55**, 11703–11712 (2021).
22. Hsu, Y. K., Chen, Y. C., Lin, Y. G., Chen, L. C. & Chen, K. H. Birnessite-type manganese oxides nanosheets with hole acceptor assisted photoelectrochemical activity in response to visible light. *J. Mater. Chem.* **22**, 2733–2739 (2012).
23. Pinaud, B. A., Chen, Z., Abram, D. N. & Jaramillo, T. F. Thin films of sodium birnessite-type MnO2: optical properties, electronic band structure, and solar photoelectrochemistry. *J. Phys. Chem. B* **115**, 11830–11838 (2011).
24. Sherman, D. M. Electronic structures of iron(III) and manganese(IV) (hydr)oxide minerals: thermodynamics of photochemical reductive dissolution in aquatic environments. *Geochim. Cosmochim. Acta.* **69**, 3249–3255 (2005).
25. Lucht, K. P. & Mendoza-Cortes, J. L. Birnessite: a layered manganese oxide to capture sunlight for water-splitting catalysis. *J. Phys. Chem. C* **119**, 22838–22846 (2015).
26. Liu, F. et al. UV–vis–infrared light driven thermocatalytic activity of octahedral layered birnessite nanoflowers enhanced by a novel photoactivation. *Adv. Funct. Mater.* **26**, 4518–4526 (2016).
27. Liu, Y. et al. Facile and green synthetic strategy of birnessite-type MnO2 with high efficiency for airborne benzene removal at low temperatures. *Appl. Catal. B: Environ.* **245**, 569–582 (2019).
28. Zia, J., Ajeer, M. & Riaz, U. Visible–light driven photocatalytic degradation of Bisphenol-a using ultrasonically synthesized polypyrrole/K-birnessite nanohybrids: experimental and DFT studies. *J. Environ. Sci.* **79**, 161–173 (2019).
29. Li, G. et al. Mn-vacancy birnessite for photo-assisted elimination of formaldehyde at ambient condition. *J. Colloid Interf. Sci.* **618**, 229–240 (2022).
30. Yang, W. et al. Insights into the surface-defect dependence of molecular oxygen activation over birnessite-type MnO_2. *Appl. Catal. B: Environ* **233**, 184–193 (2018).
31. Deibert, B. J. et al. Surface and structural investigation of a MnO_x birnessite-type water oxidation catalyst formed under photocatalytic conditions. *Chem. Eur. J* **21**, 14218–14228 (2015).
32. Zhou, S. et al. Degradation of methylene blue by natural manganese oxides: kinetics and transformation products. *R. Soc. Open Sci.* **6**, 190351 (2019).
33. Ristig, S., Cibura, N. & Strunk, J. Manganese oxides in heterogeneous (photo)catalysis: possibilities and challenges. *Green* **5**, 23–41 (2015).
34. Lee, H. & Choi, W. Photocatalytic oxidation of arsenite in TiO_2 suspension: kinetics and mechanisms. *Environ. Sci. Technol.* **36**, 3872–3878 (2002).
35. Ryu, J. & Choi, W. Photocatalytic oxidation of arsenite on TiO_2: understanding the controversial oxidation mechanism involving superoxides and the effect of alternative electron acceptors. *Environ. Sci. Technol.* **40**, 7034–7039 (2006).
36. Ying, C. et al. Highly enhanced oxidation of arsenite at the surface of birnessite in the presence of pyrophosphate and the underlying reaction mechanisms. *Water Res.* **187**, 116420 (2020).
37. Elzinga, E. J. Reductive Transformation of birnessite by aqueous Mn(II). *Environ. Sci. Technol.* **45**, 6366–6372 (2011).
38. Zhang, N. et al. Rechargeable aqueous zinc-manganese dioxide batteries with high energy and power densities. *Nat. Commun.* **8**, 405 (2017).
39. Klewicki, J. & Morgan, J. Dissolution of β-MnOOH particles by ligands: pyrophosphate, ethylenediaminetetraacetate, and citrate. *Geochim. Cosmochim. Acta* **63**, 3017–3024 (1999).
40. Klewicki, J. K. & Morgan, J. J. Kinetic behavior of Mn(III) complexes of pyrophosphate, EDTA, and citrate. *Environ. Sci. Technol.* **32**, 2916–2922 (1998).

41. Kostka, J. E., Luther, G. W. III & Nealson, K. H. Chemical and biological reduction of Mn(III)-pyrophosphate complexes: potential importance of dissolved Mn(III) as an environmental oxidant. *Geochim. Cosmochim. Acta* **59**, 885–894 (1995).
42. Salomone, V. N., Meichtry, J. M., Zampieri, G. & Litter, M. I. New insights in the heterogeneous photocatalytic removal of U(VI) in aqueous solution in the presence of 2-propanol. *Chem. Eng. J.* **261**, 27–35 (2015).
43. Wang, J. et al. Tunable mesoporous g-C_3N_4 nanosheets as a metal-free catalyst for enhanced visible-light-driven photocatalytic reduction of U(VI). *Chem. Eng. J.* **383**, 123193 (2020).
44. Nosaka, Y. & Nosaka, A. Y. Generation and detection of reactive oxygen species in photocatalysis. *Chem. Rev.* **117**, 11302–11336 (2017).
45. Wu, D., Zong, Y., Tian, Z. & Shao, B. Role of reactive oxygen species in As(III) oxidation by carbonate structural Fe(II): a surface-mediated pathway. *Chem. Eng. J.* **368**, 980–987 (2019).
46. Dutta, P. K., Pehkonen, S. O., Sharma, V. K. & Ray, A. K. Photocatalytic oxidation of arsenic(III): evidence of hydroxyl radicals. *Environ. Sci. Technol.* **39**, 1827–1834 (2005).
47. Hong, J., Liu, L., Ning, Z., Liu, C. & Qiu, G. Synergistic oxidation of dissolved As(III) and arsenopyrite in the presence of oxygen: formation and function of reactive oxygen species. *Water Res.* **202**, 117416 (2021).
48. Dou, X., Mohan, D. & Pittman, C. U. Jr Arsenate adsorption on three types of granular schwertmannite. *Water Res.* **47**, 2938–2948 (2013).
49. Shahid, M. K., Phearom, S. & Choi, Y. G. Synthesis of magnetite from raw mill scale and its application for arsenate adsorption from contaminated water. *Chemosphere* **203**, 90–95 (2018).
50. Prabhu, S. M., Kancharla, S., Park, C. M. & Sasaki, K. Synthesis of modulator-driven highly stable zirconium-fumarate frameworks and mechanistic investigations of their arsenite and arsenate adsorption from aqueous solutions. *Cryst. Eng. Comm.* **21**, 2320–2332 (2019).
51. Long, G., Peng, Y. & Bradshaw, D. A review of copper–arsenic mineral removal from copper concentrates. *Mine. Eng.* **36–38**, 179–186 (2012).
52. Luo, T., Cui, J., Hu, S., Huang, Y. & Jing, C. Arsenic removal and recovery from copper smelting wastewater using TiO_2. *Environ. Sci. Technol.* **44**, 9094–9098 (2010).
53. Qin, M., Zhao, H., Yang, W., Zhou, Y. & Li, F. A facile one-pot synthesis of three-dimensional microflower birnessite (δ-MnO_2) and its efficient oxidative degradation of rhodamine B. *RSC Adv.* **6**, 23905–23912 (2016).

Acknowledgements

Financial supports from National Natural Science Foundation of China (21876172), the “Youth Innovation Promotion Association CAS” (2020423), and the Key Laboratory Project of Gansu Province (1309RTSA041).

Author contributions

P.L.: Project administration, Supervision, Writing - original draft, Writing - review & editing; Y.W.: Investigation, Methodology; J.W.: Methodology, Formal analysis, Data curation; W.W.: Software; Z.D.: Visualization; J.L.: Validation; Q.F.: Conceptualization, Resources, Funding acquisition.

Competing interests

The authors declare no competing interests.

Additional information

Supplementary information The online version contains supplementary material available at https://doi.org/10.1038/s41545-024-00316-7.

Correspondence and requests for materials should be addressed to Qiaohui Fan.